

Deep Network Uncertainty Maps for Indoor Navigation

Francesco Verdoja*, Jens Lundell* and Ville Kyrki

Abstract—Most mobile robots for indoor use rely on 2D laser scanners for localization, mapping and navigation. These sensors, however, cannot detect transparent surfaces or measure the full occupancy of complex objects such as tables. Deep Neural Networks have recently been proposed to overcome this limitation by learning to estimate object occupancy. These estimates are nevertheless subject to uncertainty, making the evaluation of their confidence an important issue for these measures to be useful for autonomous navigation and mapping. In this work we approach the problem from two sides. First we discuss uncertainty estimation in deep models, proposing a solution based on a fully convolutional neural network. The proposed architecture is not restricted by the assumption that the uncertainty follows a Gaussian model, as in the case of many popular solutions for deep model uncertainty estimation, such as Monte-Carlo Dropout. We present results showing that uncertainty over obstacle distances is actually better modeled with a Laplace distribution. Then, we propose a novel approach to build maps based on Deep Neural Network uncertainty models. In particular, we present an algorithm to build a map that includes information over obstacle distance estimates while taking into account the level of uncertainty in each estimate. We show how the constructed map can be used to increase global navigation safety by planning trajectories which avoid areas of high uncertainty, enabling higher autonomy for mobile robots in indoor settings.

I. INTRODUCTION

Deep Neural Networks (DNNs) have recently found increased adoption in robotics, where they are being proposed for applications such as grasping [1] and autonomous navigation [2]. This is, however, raising concerns over Artificial Intelligence (AI) safety [3], especially in situations where unreliable predictions can cause damage to expensive hardware or even human harm, as in the case of recent accidents involving autonomous vehicles, where in May 2016 the perception system in a car failed to recognize the presence and distance of an obstacle which unfortunately ended in a fatal crash. In order to integrate Deep Learning (DL) into applications, it is therefore important that such systems are able to produce reliable estimates of the uncertainty associated with their predictions.

Autonomous navigation of mobile robots is one of the areas where AI safety is of utmost importance, both in regards to autonomous cars and to robots designed to be employed in industrial settings, since the robots are often big enough to potentially damage the environment or harm the users. Autonomous cars often employ a wide array of

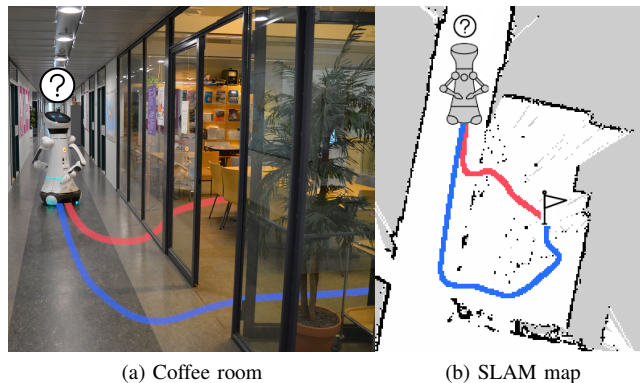


Fig. 1. Two possible navigation trajectories that a robot relying only on 2D lidar could plan to reach a goal. The blue trajectory is longer but safe, while the red one would result in a collision with the glass walls of the room (best viewed in color).

sensors to estimate the state of their surroundings while most indoor mobile robots rely only on 2D laser scanners for navigation, mapping and localization as they provide distance measurements at fast rates and in wide angular fields [4]. However, 2D laser scans offer a limited amount of information that may be insufficient for tasks like object detection and obstacle avoidance. In particular, 2D lidars are not able to detect transparent obstacles, *e.g.*, glass, and are limited to measuring occupancy at a single height and therefore cannot infer the true occupancy of complex objects such as tables. For example, Figure 1 shows two trajectories planned on a map built using 2D lidars only; a robot could not determine that the red path would collide with the glass walls of the room shown in Figure 1a as they are invisible to the laser scanners.

To overcome these limitations, we recently proposed a virtual laser-like sensor, using a convolutional network trained to infer, or *hallucinate*, the actual distance of objects from raw 2D laser input [5]. We refer to this distance as the *robot-to-obstacle distance*, *i.e.*, “the distance along a certain direction to the closest point of an obstacle that the robot could collide with.” We demonstrated in that work the ability of the approach to estimate the occupancy of complex objects (*e.g.*, tables and glass walls), and how it could improve safety for local navigation, while its applications to global navigation and mapping was left unexplored.

Using such a sensor for mapping would allow building maps which account for actual obstacle occupancy and could yield safer navigation when compared to those built by using laser data alone. However, when building occupancy grid maps from laser data, the sensor uncertainty is so low to

*These authors contributed equally to this paper.

This work was supported by the Strategic Research Council at Academy of Finland, decision 314180.

F. Verdoja, J. Lundell and V. Kyrki are with School of Electrical Engineering, Aalto University, Finland. `name.surname@aalto.fi`

fall inside the grid resolution and for that reason is usually neglected. This is not the case for robot-to-obstacle distance estimates: the network uncertainty is too wide to ignore and for that reason it has to be accounted for while mapping.

Therefore, in this work we propose to model the uncertainty of the convolutional network in [5] and exploit the model to build uncertainty maps. Figure 6d shows an example of such a map, where trajectories can be planned to avoid areas of high uncertainty—marked in red—resulting in safer paths.

The most widely adopted approach to predict uncertainty of deep models is known as Monte-Carlo (MC) Dropout [6]. However, it has been shown that the application of MC Dropout to some domains can be problematic [7]–[9], and we demonstrate how it cannot be used effectively for the task at hand. We then propose an alternative DL-based method which is able to produce adequate prediction of uncertainty.

The main contributions of this study are: (1) a novel DL-based approach for uncertainty prediction (Section III-A and Section III-B) and its application in the domain of robot-to-obstacle distance estimation from raw 2D laser data; (2) an algorithm for building uncertainty maps of indoor environments (Section III-C) that can be used to integrate uncertainty predictions in global navigation frameworks; (3) an empirical comparison of the proposed technique with the de-facto standard MC Dropout for the task at hand, showing how the proposed approach is a superior choice in this domain (Section IV).

II. RELATED WORKS

A. Uncertainty in robotic mobility

In the context of robotic mobility, we recognize three different areas where recent research addressed uncertainty: (1) localization, where the goal is to reduce uncertainty regarding the robot position in relation to a known environment; (2) local navigation, where robot movements should account for sensor uncertainty over obstacle position and occupancy; and (3) mapping and global navigation, where planned trajectories should avoid areas whose content is uncertain, and prefer obstacle-free paths a robot can safely navigate. Here, we only review (2) and (3) as they are central for our work, but we encourage readers interested in (1) to read, *e.g.*, [10], [11].

a) Local navigation: Ensuring safety in the context of local navigation requires to estimate from sensory data the position and occupancy of obstacles surrounding the robot. To achieve this task robots often rely on raw 2D laser data, despite laser sensors inherent limitation in providing correct distance estimates for many complex objects, including tables, chairs, windows, and open shelves. A recent paper [12] presented a method for planning theoretically safe paths in environments sensed by a 2D lidar. The authors proposed to inflate obstacles by a volume that represented both the pose uncertainty and the space the obstacle may occupy. However, the experimental demonstration was limited to simple objects and nothing was advised for tackling more complex objects. Another option to reduce obstacle uncertainty is sensor

fusion [4], [13], but such approaches typically require visual sensors that suffer from limited field of view and higher processing time.

We recently shifted the focus from estimating obstacle occupancy from raw 2D laser data towards learning to infer robot-to-obstacle distances using neural networks [5]. The results demonstrated first of all that typical indoor environments include enough structure to learn the robot-to-obstacle distance of objects such as tables and windows, and secondly that the learned robot-to-obstacle distance can improve local navigation safety. However, that work did not address obstacle position uncertainty, but rather focused on situations where raw laser readings could not capture the actual robot-to-obstacle distance and in those cases tried to produce better estimates. In this paper, on the other hand, we address the problem of predicting the uncertainty over the deep model used to produce the robot-to-obstacle distance and show how to integrate this information when building maps.

b) Mapping and global navigation: Indoor environments are often represented as occupancy grid maps, where each cell represents a portion of the environment that is either free, occupied or unknown. When a robot has to plan a path to a particular pose, it searches for a trajectory through the free space that reaches the goal position at a minimum cost, according to a predefined cost function. Usually, the grid maps are built through accumulation of evidence by running the robot in the environment. This process naturally lends itself to account for uncertainty, as effectively each cell contains the belief of it being occupied. However, occupancy maps are normally thresholded and used in the aforementioned ternary form [14]. Uncertainty is then accounted for in different ways, *e.g.*, through planning in a belief state over obstacle positions to minimize path uncertainty [15] or by inflating or deflating obstacles depending on collision probability [16].

A recent paper presented a method for fusing measurement uncertainty directly into the map [17]. That work, however, assumed uncertainty stemmed from noisy measurement and not from the inability to detect the occupancy of objects in the environment. Whereas in this work it is defined as the uncertainty of a deep model estimating robot-to-obstacle distances. This enables building uncertainty maps that not only contain actual object occupancies but also their positional uncertainty. Here, we present a method for building such maps which is a step forward from ternary occupancy maps.

B. Deep model uncertainty

Standard DL architectures provide point estimates, but do not inherently capture model uncertainty. Uncertainty can, however, be evaluated with Bayesian Neural Networks (BNNs) [18], [19] where deterministic weights are replaced with distributions over the parameters. Although BNNs are relatively easy to formulate, using them to perform inference is unfeasible as it is often intractable to analytically evaluate the marginal probability required for training. Recent new

variational inference methods have been proposed to address this issue, but they still come with increased computational cost, requiring in most cases to double the number of parameters of a network to represent its uncertainty [6], [20].

Another possibility to model uncertainty in DNNs that has attracted a lot of interest recently is to use dropout as approximate Bayesian variational inference [6]. The key idea is to enable dropout not only in training but also during testing, do several forward passes through the network with the same input data, and as a final step estimate the first two moments (mean and variance) of the predictive distribution. The mean is then used as the estimate, and the variance as a measure of uncertainty. Using this approach, researchers have increased semantic segmentation performance on images [21] and visual relocalization accuracy [22]. Despite the success of using MC Dropout to estimate uncertainty in deep models, there are scenarios where the approach does not generate reasonable results [7]–[9]. In particular, analysis by Osband [8] indicates that the variance from MC Dropout is correlated with the predicted mean. In Section IV, we provide experimental evidence for this effect, which prevents the use of MC Dropout in the context of this work, where the impact of the mean on the variance estimate is strong.

III. METHOD

In this section, we describe an approach for predicting uncertainty of distance estimates and how to integrate it when building occupancy maps. Following the formalism presented in [5], let us define the output of a generic N -point 2D laser positioned at a height h from floor level as a 1D vector $\mathbf{l}_h = \{l_{ih}\}_{i=1}^N$ where each l_{ih} represents an estimate (usually, in meters) of the distance d_{ih} of closest obstacle from the laser at height h , along the direction i . When considering a specific robot with height H and a 2D laser sensor positioned at a fixed height $h^* \in [0, H]$, we define the vector $\mathbf{x} = \mathbf{l}_{h^*}$. The robot-to-obstacle distances are represented as the closest point along each direction,

$$\mathbf{y} = \{y_i \mid y_i = \min_{h \in [0, H]} d_{ih}\}_{i=1}^N. \quad (1)$$

Let $\hat{\mathbf{y}}$ be an estimate of \mathbf{y} , given from a function approximator \mathcal{H} that takes raw 2D laser signal \mathbf{x} as input. Such a function approximator was introduced in our original work [5]. In this work, we develop a method to predict the uncertainty of the estimator \mathcal{H} .

A. Uncertainty models

Assuming independence between each data point, the likelihood that $\hat{\mathbf{y}} = \mathcal{H}(\mathbf{x})$ follows a parametric model with parameters θ is

$$\mathcal{L}(\hat{\mathbf{y}} \mid \theta) = \prod_{i=1}^N p(\hat{y}_i \mid \theta). \quad (2)$$

We are interested in a model that maximizes \mathcal{L} , or, more practically, the log-likelihood $\ell(\hat{\mathbf{y}} \mid \theta) = \ln \mathcal{L}(\hat{\mathbf{y}} \mid \theta)$. A common choice is to assume the uncertainty follows a Gaussian model, as in the case of MC Dropout [6], [23].

Under that assumption, one can center the distribution on the true robot-to-obstacle distance y_i and represent the uncertainty using the model standard deviation by finding an uncertainty vector $\hat{\mathbf{u}} = \{\hat{u}_i\}_{i=1}^N$ such that $\hat{\mathbf{u}} = \arg \max_{\hat{\mathbf{u}} \in \mathbb{R}_+^N} \ell_{\mathcal{N}}(\hat{\mathbf{y}} \mid \mathbf{y}, \hat{\mathbf{u}})$, where

$$\begin{aligned} \ell_{\mathcal{N}}(\hat{\mathbf{y}} \mid \mathbf{y}, \hat{\mathbf{u}}) &= \sum_{i=1}^N \ln p(\hat{y}_i \mid \mu = y_i, \sigma = \hat{u}_i) \\ &= \sum_{i=1}^N \ln \left(\frac{1}{\sqrt{2\pi}\hat{u}_i} \exp \left(-\frac{(\hat{y}_i - y_i)^2}{2\hat{u}_i^2} \right) \right) \\ &= -\frac{1}{2} \sum_{i=1}^N \left(\ln 2\pi\hat{u}_i^2 + \frac{(\hat{y}_i - y_i)^2}{\hat{u}_i^2} \right). \end{aligned} \quad (3)$$

However, as we will demonstrate in Section IV such a model is unable to correctly represent the data considered in this work.

Another option is to assume the uncertainty follows a Laplace distribution, a choice that was shown to work well for estimating uncertainty in regression tasks in vision [23]. In this case the uncertainty is represented by the scale parameter b of the Laplace distribution by finding $\hat{\mathbf{u}} = \arg \max_{\hat{\mathbf{u}} \in \mathbb{R}_+^N} \ell_L(\hat{\mathbf{y}} \mid \mathbf{y}, \hat{\mathbf{u}})$, where

$$\begin{aligned} \ell_L(\hat{\mathbf{y}} \mid \mathbf{y}, \hat{\mathbf{u}}) &= \sum_{i=1}^N \ln p(\hat{y}_i \mid \mu = y_i, b = \hat{u}_i) \\ &= \sum_{i=1}^N \ln \left(\frac{1}{2\hat{u}_i} \exp \left(-\frac{|\hat{y}_i - y_i|}{\hat{u}_i} \right) \right) \\ &= -\sum_{i=1}^N \left(\ln 2\hat{u}_i + \frac{|\hat{y}_i - y_i|}{\hat{u}_i} \right). \end{aligned} \quad (4)$$

B. Network architecture

We propose to train a DNN \mathcal{U} to estimate $\hat{\mathbf{u}}$. Figure 2 shows schematically the proposed architecture. The network is divided in two components. The first is an encoder φ that takes as input a 2D matrix of length $N = 128$ obtained by concatenating \mathbf{x} and $\hat{\mathbf{y}}$ over the second dimension. It then passes this 128×2 input through four 1D convolutional layers (kernel size $K = 5$, stride $S = 2$), connected via Batch Normalization (BN) [24] and Rectified Linear Unit (ReLU) [25] layers. The output sizes of the convolutional layers are, in order, 64×16 , 32×32 , 16×64 , and 8×128 . The output of φ is the input to the second part of the network: the decoder ψ , which has the same structure as φ , and outputs a 1D vector $\hat{\mathbf{u}}$ of size N through a series of 1D transposed deconvolutional layers ($K = 5$, $S = 2$), also connected via BN and ReLU. The size of the layers' outputs are the opposite to the encoder's, *i.e.*, 16×64 , 32×32 , 64×16 , and 128×1 . Corresponding convolutional and deconvolutional layers are connected through skip connections, as their ability to improve the performance of the network has been demonstrated in this domain [5]. The input of the network is scaled to the range $[0, 1]$ to improve convergence speed, and weights are optimized using Adaptive Moment Estimation (Adam).

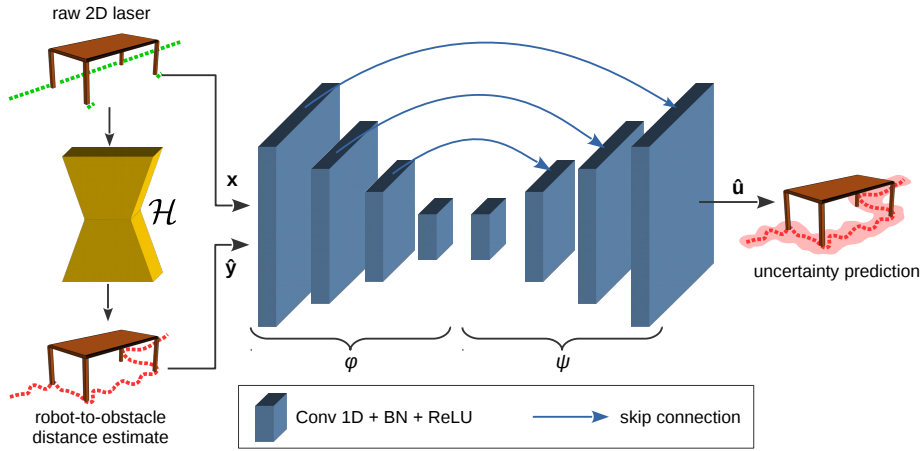


Fig. 2. The proposed fully convolutional network \mathcal{U}

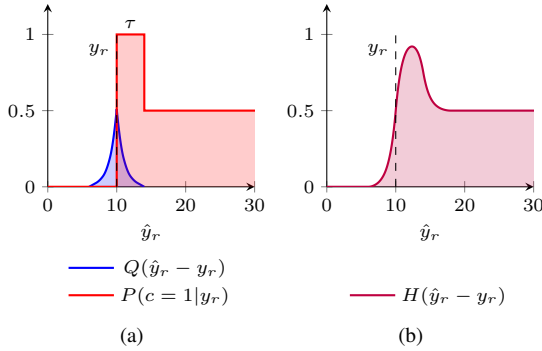


Fig. 3. The geometric construction of $P(c = 1|y_r)$, where τ equals half the support of Q (a), and the resulting convolution (b).

Depending on which uncertainty (Gaussian or Laplacian) the network should model, the loss function it minimizes is either the negative log-likelihood of (3) or (4). Although in this work we limit the study to those two models, the proposed method can work with any other parametric distribution.

C. Building an uncertainty map

Next we present a method for building occupancy maps that incorporates both the robot-to-obstacle distance prediction and its uncertainty. To create these maps—which we call *uncertainty maps*—we adapt standard occupancy mapping techniques [14] to account for our uncertainty estimates similarly to [17], [26]. In the following, we will present the construction for an uncertainty model following a Laplacian distribution; however, the construction for a Gaussian model is similar and is discussed in detail in [17].

The occupancy probability $P(c = 1|\hat{y}_r)$ of a cell c given an estimated robot-to-obstacle distance \hat{y}_r along a laser ray r is defined as

$$P(c = 1|\hat{y}_r) = \int_0^\infty P(c = 1|y_r)P(y_r|\hat{y}_r) dy_r, \quad (5)$$

where y_r represents the true robot-to-obstacle distance along ray r . Here, we model the occupancy given the true robot-to-obstacle distance $P(c = 1|y_r)$ as 0 in front of the obstacle, 1

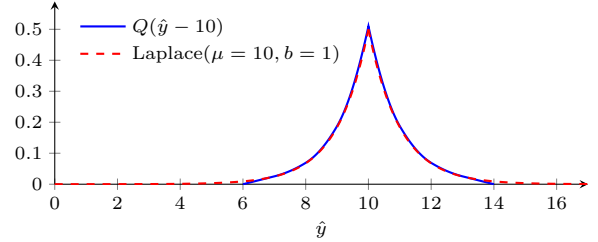


Fig. 4. The quadratic B-spline function Q , and the corresponding Laplace

from the surface to τ units behind, and then 0.5. An example of $P(c = 1|y_r)$ is shown in red in Figure 3a.

Calculating the integral in (5) requires a model $P(y_r|\hat{y}_r)$ of the true robot-to-obstacle distance given a noisy measurement reading. As stated in Section III, $P(y_r|\hat{y}_r)$ is modeled as a Laplace distribution. However, as pointed out in [26], integrating (5) over a distribution with infinite support results in obstacles lying slightly behind the range measurement even when the measurements are precise. One solution is to set $\tau = \infty$, but this can degenerate occupancy probabilities [26]. Another, more stable option, is to limit the support of $P(y_r|\hat{y}_r)$. In this work, similarly to [26], the support of a Laplace distribution is limited by approximating it as a quadratic B-spline $Q(t) \approx P(y_r|\hat{y}_r)$ where $t = (y_r - \hat{y}_r)/\hat{u}_r$ and $\hat{u}_r = \mathcal{U}(x_r, \hat{y}_r)$. We derived Q numerically by imposing it to have finite support $[-4, 4]$ and unit integral. The choice of the range for the support originates from the fact that, for a $\text{Laplace}(0, 1)$, around 99% of the cumulative distribution lies in that range. Figure 4 shows the resulting spline approximation.

By choosing the thickness term $\tau = 4\hat{u}_r$, i.e., half the support of the approximated B-spline, (5) has the analytical solution

$$P(c = 1|\hat{y}_r) \approx H(t) = Q_{\text{cdf}}(t) - \frac{1}{2}Q_{\text{cdf}}(t - 4), \quad (6)$$

where $Q_{\text{cdf}}(t)$ is the cumulative density function of the quadratic B-spline $Q(t)$. The per-ray occupancy probability is visualized in Figure 3b.

Algorithm 1 Uncertainty Map

Inputs: \mathbf{P} : Robot poses, \mathbf{L} : Laser scans,
 \mathbf{M} : Empty map, α : Correlation factor.

```
for all  $p \in \mathbf{P}$  do  
   $\mathbf{x} \leftarrow \text{GETLASERSCAN}(\mathbf{L}, p)$   
   $\hat{\mathbf{y}} \leftarrow \mathcal{H}(\mathbf{x})$   
   $\hat{\mathbf{u}} \leftarrow \mathcal{U}(\mathbf{x}, \hat{\mathbf{y}})$   
  for all  $r \in 1, \dots, N$  do  
     $\mathbf{C} \leftarrow \text{RAYCAST}(p, \hat{\mathbf{y}}_r)$   
    for all ( $c \in \mathbf{C}$ ) do  
       $d_{c\hat{y}_r} \leftarrow \text{EUCLIDDIST}(c, \hat{\mathbf{y}}_r)$   
       $o_c \leftarrow H\left(\frac{d_{c\hat{y}_r} - \hat{y}_r}{\hat{u}_r}\right)$   
       $m_c \leftarrow \log \frac{o_c}{1 - o_c}$   
       $\mathbf{M}(c) \leftarrow \mathbf{M}(c) + \alpha m_c$   
    end for  
  end for  
end for  
return  $\frac{1}{1 + \exp(\mathbf{M})}$ 
```

The method for creating uncertainty maps with occupancy probabilities calculated in (6) is summarized in Algorithm 1. We assume robot poses \mathbf{P} and original laser scans \mathbf{L} to be given. First for each robot pose p , the algorithm extracts the associated original laser scan \mathbf{x} . This laser scan is then propagated through network \mathcal{H} to estimate the robot-to-obstacle distance $\hat{\mathbf{y}}$ which, together with the original laser, is propagated through \mathcal{U} to estimate the scale parameters $\hat{\mathbf{u}}$ of the Laplacian uncertainty model. Next, the algorithm goes through every laser ray \hat{y}_r in the current scan $\hat{\mathbf{y}}$ and finds all cells \mathbf{C} that are touched by the laser ray r originating from the current pose p . Then the algorithm iterates over each cell $c \in \mathbf{C}$, calculates the distance $d_{c\hat{y}_r}$ between the center of the cell and the estimated obstacle distance \hat{y}_r , calculates the occupancy for that cell using (6) with $t = (d_{c\hat{y}_r} - \hat{y}_r) / \hat{u}_r$, converts the occupancy to *log-odds*, scales it with a correlation factor α , and finally adds it to the previous occupancy value for that cell. As a final step the uncertainty map \mathbf{M} is converted from log-odds to occupancy probability, *i.e.*, in $[0, 1]$.

The correlation factor $0 < \alpha < 1$ limits the effect for which highly correlated readings could produce overconfident maps and remove most of the uncertainty. This parameter should be set as a function of the amount of correlation between successive readings; in this work we experimentally set it to a constant value $\alpha = 0.01$ as we are working in a static environment. In a dynamic environment, α can be set as a function of the time passed between readings to have the map adapt to changes in the environment [17].

IV. EXPERIMENTS

In this work, we propose a framework for building uncertainty maps based on deep network uncertainty models. Evaluation of the proposed approach is then two-fold: first of all we are interested in assessing the quality of the

TABLE I
AVERAGE LOG-LIKELIHOOD OVER THE VALIDATION SETS

| Algorithm | Model | Val2F | Val3F |
|------------|----------|-------------|-------------|
| MC Dropout | Gaussian | -2.55 | -4.63 |
| Ours | Gaussian | -1.42 | 1.48 |
| Ours | Laplace | 1.65 | 3.25 |

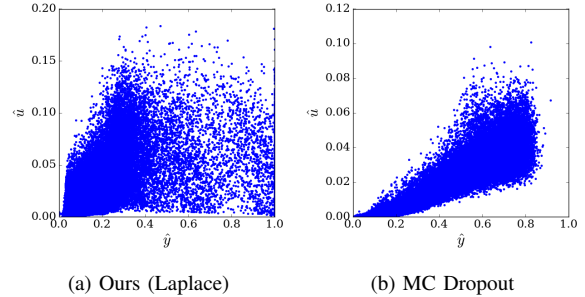


Fig. 5. Plots of the relationship between the estimated robot-to-obstacle distance $\hat{\mathbf{y}}$ and uncertainty $\hat{\mathbf{u}}$ for the proposed method and MC Dropout.

proposed uncertainty model (Section IV-B); secondly, we want to analyze the resulting uncertainty maps to validate the suggested mapping strategy (Section IV-C). However, for completeness, we first present the network training setup.

A. Dataset and network training

We used the trained network \mathcal{H} , whose training setup was detailed in [5]. Then, to train the uncertainty network \mathcal{U} , we took the complete training and test set used in [5], available online¹, and merged them. These two datasets were gathered in a university building, on the second and third floor, respectively, and once merged consisted of 39508 pairs of laser scan \mathbf{x} (input of \mathcal{H}) and relative robot-to-obstacle distance \mathbf{y} (ground-truth output). We propagated each laser scan \mathbf{x} through the trained network \mathcal{H} , saved each pair $(\mathbf{x}, \hat{\mathbf{y}})$ as training input for \mathcal{U} , and kept \mathbf{y} as ground-truth data to compute the loss as explained in Section III-B. We saved these new input-output pairs as a new dataset we used to train network \mathcal{U} . The reason for merging the two datasets is that the errors produced by \mathcal{H} over the training set differs slightly compared to the test set, due to the training process; thus, merging the two datasets enable us to capture a wider range of uncertainties while training \mathcal{U} while limiting overfitting. The network was trained for 2000 epochs, with a batch size of 32, and learning rate set to 10^{-4} .

For validation, we gathered new data by teleoperating a Care-O-bot 4 in the same environments where the previous datasets were gathered. This resulted in two new datasets, which we will refer to as Val2F and Val3F. Val2F consists of 18961 samples gathered on the second floor while Val3F consists of 24829 samples from the third floor. By performing a new acquisition we ensure that we conduct our evaluation on data which is uncorrelated with the training set.

¹github.com/jsll/IROS2018-Hallucinating-Robots

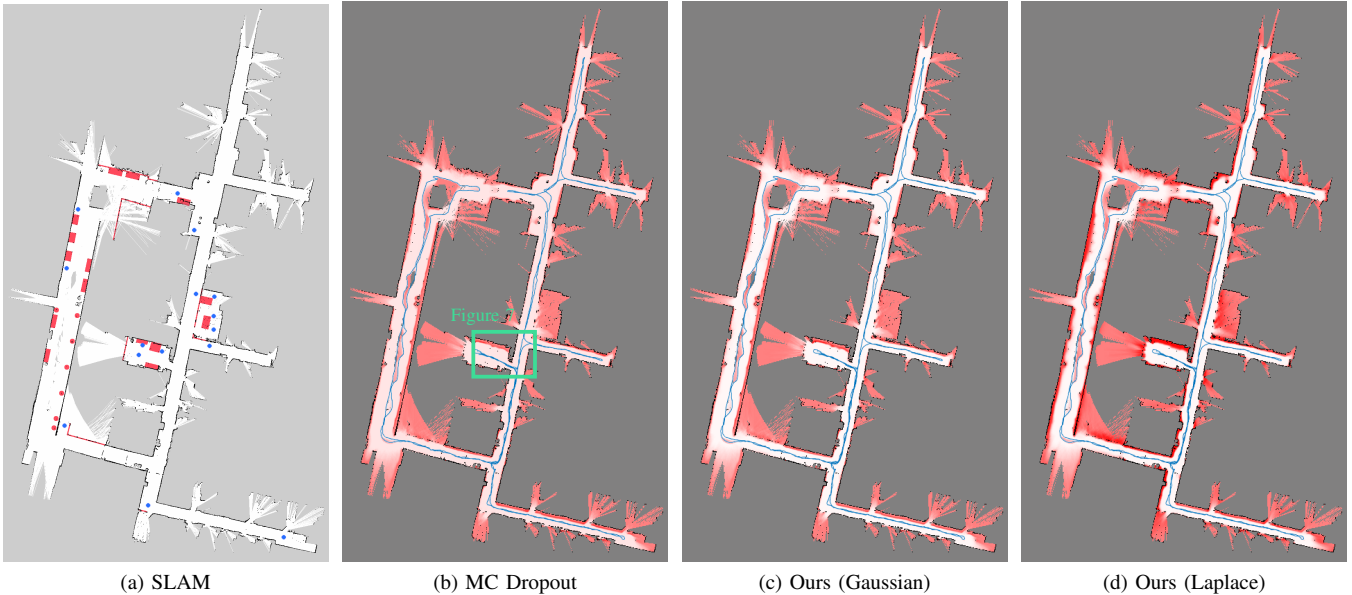


Fig. 6. The maps created by gathering data with a Care-O-bot 4. In (a) the obstacles invisible to the laser scanner are indicated in red, and the 15 navigation goals used in the navigation experiment in blue. In all other figures, the original SLAM map is visualized in gray scale while the superimposed uncertainty maps shown in degrees of red. As in regular occupancy maps, darker red indicates a higher occupancy probability. The blue line is the robot path (best viewed in color).

B. Model quality evaluation

To evaluate the quality of the proposed uncertainty model we compare its performance to that obtained by state-of-the-art MC Dropout [6]. To obtain MC Dropout’s results we modified the network in [5] to include dropout layers after each convolutional layer. We will refer to this modified version of \mathcal{H} as \mathcal{H}_D . We then trained the network with a dropout rate of 50%. In testing, to evaluate uncertainty, we performed 50 forward passes of the same input in the network using the same dropout rate. We then took the average of this sampling process as the network prediction for the robot-to-obstacle distance \hat{y} and the variance of the samples as the estimated uncertainty \hat{u} , as proposed in [6].

Table I shows average log-likelihood scores over the two validation sets for our approach, both using Gaussian and Laplacian models, and MC Dropout. It is noticeable that both methods using Gaussian model are unable to correctly model uncertainty of robot-to-obstacle distances and get considerably lower scores than our approach using Laplacian model. This makes it impossible to use an approach like MC Dropout for the application at hand; given that it assumes by design the uncertainty to be Gaussian. Our approach instead, given its ability to be optimized for any distribution, can be used effectively, *e.g.*, by selecting a Laplacian model.

Moreover, Figure 5 presents plots examining the relationship between the estimated robot-to-obstacle distance \hat{y} (horizontal axis) and the relative predicted uncertainty \hat{u} (vertical axis) for both our approach and MC Dropout. Each plot represents results over the whole Val2F set where each point corresponds to one lidar distance reading. It is apparent from Figure 5b that for MC Dropout a strong correlation between \hat{u} and \hat{y} is manifested. Given the lidar sensor, this

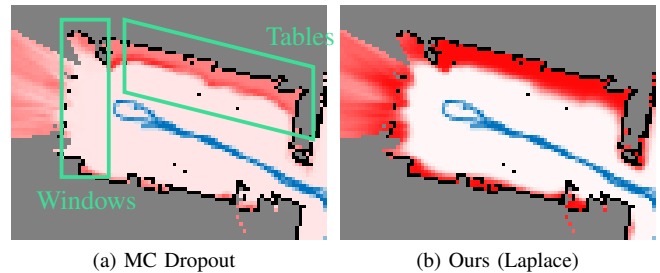


Fig. 7. Marked area in Figure 6b (best viewed in color).

should not be the case: the uncertainty should be independent of the distance at which the obstacle lays. As seen in Figure 5a, no similar effect is present for our model. This side-effect of MC Dropout, which was theoretically noted in [8], is therefore confirmed by our empirical evaluation, demonstrating that the use of MC Dropout may not be suitable for domains, like the one at hand, where there is a wide range of possible output values and where therefore the dependence of MC Dropout’s variance from the estimated mean overshadows any other contribution.

C. Uncertainty maps

Building an uncertainty map requires robot poses, laser scans, and the inverse measurement model. To collect these we first teleoperated a Care-O-bot 4 in our facility to gather odometry and laser range data, then we built the SLAM map shown in Figure 6 using ROS gmapping, and finally we ran ROS amcl² to register robot poses depicted as the blue path

²gmapping: <http://wiki.ros.org/gmapping>,
amcl: <http://wiki.ros.org/amcl>

in Figure 6.

Once laser measurements and odometry were collected, we created, in addition to the base SLAM map, three other maps: a map obtained using MC Dropout (Figure 6b), and two different maps using our proposed approach, one modeling the uncertainty as a Gaussian distribution (Figure 6c) and another one modeling it as a Laplace (Figure 6d). All three maps were created using Algorithm 1 with $\alpha = 0.01$, where the only difference were in determining $\hat{\mathbf{u}}$. In the maps depicted in Figures 6c and 6d $\hat{\mathbf{u}}$ was set as the output from the uncertainty network, while for the MC Dropout map in Figure 6b $\hat{\mathbf{u}}$ was set as the standard deviation of the outputs obtained from 50 forwards passes of the same input through network \mathcal{H}_D .

A magnified sections of these maps are shown in Figure 7. From visually inspecting the figure one can conclude that the uncertainty maps (visualized as the red shaded area) are coherent with the original SLAM map in areas with low uncertainty such as for walls, while differing in less certain areas which includes windows and tables. Although our Gaussian uncertainty map and the MC Dropout map are very similar, the main difference is that the MC Dropout map is more uncertain about cells that are clearly free including the robot path.

With regards to the map in Figure 6b produced by MC Dropout, it is worth noticing that although the map looks reasonable thanks to the good estimate of the distance, the estimate of the uncertainty in that map is inaccurate, as demonstrated in Section IV-B. This causes the map to underestimate the occupancy of obstacles: given the correlation between the uncertainty and the estimated distance (see Figure 5b): when the robot is very close, any estimate is taken as certain. This is apparent in particular in Figure 7, where the MC Dropout map cannot capture the occupancy of tables nor windows, which our Laplace map estimates correctly.

D. Global navigation on uncertainty maps

To test the ability of uncertainty maps to improve global navigation safety, we run a simulation experiment where we left a robot randomly navigate an environment with and without uncertainty maps. More precisely, we setup a Gazebo simulation mirroring the real Val2F environment, we then had a robot plan a sequence of 400 trajectories each connecting two points from a set of 15 goal points distributed over the environment³. The path planning was performed by using standard ROS gmapping. We repeated the experiment changing each time the costmap used by gmapping to include the SLAM map and either one of the three uncertainty maps in Figure 6. As baseline, we ran the same navigation using only a SLAM map without uncertainty. We manually marked in the environment occupancy of objects invisible to the laser (*e.g.*, table, benches and glass walls) and then computed the number of time a navigation path would collide with any

³The code for the navigation experiment is available for download at github.com/aalto-intelligent-robotics/uncertain_turtlebot_navigation

TABLE II
NUMBER OF PATH RESULTING IN COLLISIONS OVER 400 TRAJECTORIES
FOR THE DIFFERENT TYPES OF MAP

| Map | Model | n. of collision | Percentage |
|------------|----------------|-----------------|--------------|
| SLAM only | no uncertainty | 23 | 5.75% |
| MC Dropout | Gaussian | 76 | 19.00% |
| Ours | Gaussian | 71 | 17.75% |
| Ours | Laplace | 0 | 0.00% |

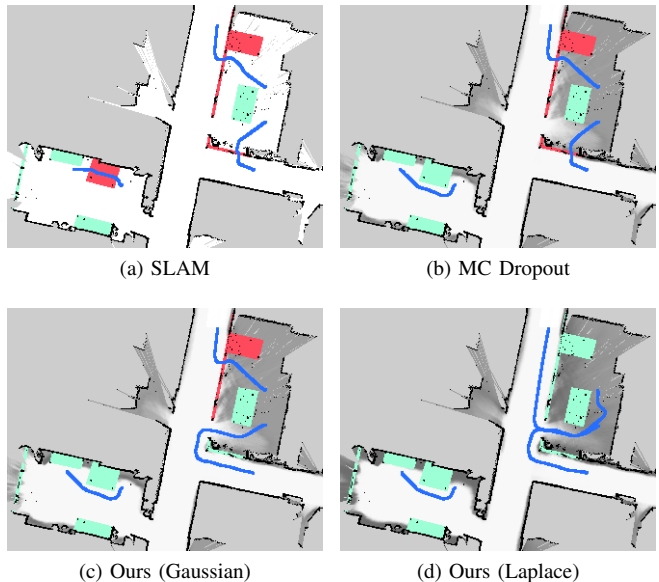


Fig. 8. Three sample navigation trajectories (blue lines) executed on four different maps. The true occupancy of objects invisible to the laser is overlaid on the maps, in green when no collision occurred or in red in case of collision. The uncertainty map is shown in shades of gray (best viewed in color).

of these obstacles when using each of the four different maps. Figure 6a shows the 15 goal points in blue and the aforementioned occupied areas in red.

Table II presents the results of this experiment, which demonstrates the benefits uncertainty maps can have on global navigation safety. However, the model of the uncertainty needs to be accurate, otherwise it might mislead the planner. As we discussed in the previous sections, Gaussian models produce overconfident predictions which resulted in even more collision compared to planning on SLAM maps alone. On the other hand, the ability of our Laplace model to correctly estimate areas of high uncertainty enabled the robot to avoid risky areas and prefer safer options, resulting in safer navigation and, in our experiment, no collisions.

Figure 8 shows an example of these trajectories. It is apparent that the path planned in our Laplace map (see Figure 8d) ends in the correct position without any risk for collisions as it plans around more uncertain areas, keeps further away from the walls, and successfully avoids the glass surface. The same is not true for all paths planned on the SLAM map (Figure 8a) and at least some of the paths planned on the other uncertainty maps (Figures 8b and 8c).

V. CONCLUSIONS

Building occupancy maps in environments full of complex obstacles is challenging but crucial for autonomous robot navigation. To this end, we presented a method for predicting model uncertainty of a deep network estimating robot-to-obstacle distance and proposed a mapping algorithm to create uncertainty maps for indoor autonomous global navigation. To achieve this we trained an uncertainty network that takes both estimated and original laser readings as inputs and outputs an uncertainty measure over the estimated distances. In the quantitative evaluation when the uncertainty network modeled uncertainties as Laplacian opposed to Gaussian it produced much better predictions in comparison to the state-of-the-art MC Dropout, indicating that wider tailed distributions are better equipped to capture uncertainties in this domain. Extension of this idea to other domains is left as future work.

The ability of the Laplacian model to better represent obstacle distances is also apparent when creating uncertainty maps, where the map built using our Laplacian strategy successfully marked otherwise invisible objects such as glass as occupied, while the map built using a Gaussian model did not capture such areas due to the overconfident uncertainty estimates. In addition, we demonstrated that paths planned on an uncertainty map prefer areas of lower uncertainty and reduce the probability of collision, increasing autonomous navigation safety over the use of traditional ternary occupancy maps.

Finally it is worth mentioning that although the proposed architecture was only tested in this domain, it is agnostic to the estimator \mathcal{H} and to the data it is processing, indicating that it may generalize to model uncertainties in other domains as well. However, generalization of this architecture is out of the scope of this study and is left as future work.

REFERENCES

- [1] J. Varley, C. DeChant, A. Richardson, J. Ruales, and P. Allen, "Shape completion enabled robotic grasping," in *2017 IEEE/RSJ International Conference on Intelligent Robots and Systems (IROS)*, Sept. 2017, pp. 2442–2447.
- [2] M. Pfeiffer, M. Schaeuble, J. Nieto, R. Siegwart, and C. Cadena, "From perception to decision: A data-driven approach to end-to-end motion planning for autonomous ground robots," in *Robotics and Automation (ICRA), 2017 IEEE International Conference on*. IEEE, 2017, pp. 1527–1533.
- [3] D. Amodei, C. Olah, J. Steinhardt, P. Christiano, J. Schulman, and D. Mané, "Concrete Problems in AI Safety," *arXiv:1606.06565 [cs]*, June 2016. [Online]. Available: <http://arxiv.org/abs/1606.06565>
- [4] H. Baltzakis, A. Argyros, and P. Trahanias, "Fusion of laser and visual data for robot motion planning and collision avoidance," *Machine Vision and Applications*, vol. 15, no. 2, pp. 92–100, Dec. 2003.
- [5] J. Lundell, F. Verdoja, and V. Kyrki, "Hallucinating robots: Inferring Obstacle Distances from Partial Laser Measurements," in *2018 IEEE/RSJ International Conference on Intelligent Robots and Systems (IROS)*. Madrid, Spain: IEEE, 2018, pp. 4781–4787.
- [6] Y. Gal and Z. Ghahramani, "Dropout As a Bayesian Approximation: Representing Model Uncertainty in Deep Learning," in *Proceedings of the 33rd International Conference on International Conference on Machine Learning*, ser. ICML'16, vol. 48, New York, NY, USA, 2016, pp. 1050–1059.
- [7] I. Osband, C. Blundell, A. Pritzel, and B. Van Roy, "Deep Exploration via Bootstrapped DQN," in *Advances in Neural Information Processing Systems 29 (NIPS 2016)*, D. D. Lee, M. Sugiyama, U. V. Luxburg, I. Guyon, and R. Garnett, Eds. Curran Associates, Inc., 2016, pp. 4026–4034.
- [8] I. Osband, "Risk versus Uncertainty in Deep Learning: Bayes, Bootstrap and the Dangers of Dropout," in *NIPS 2016 Workshop on Bayesian Deep Learning*, Barcelona, Spain, Dec. 2016.
- [9] T. Pearce, N. Anastassacos, M. Zaki, and A. Neely, "Bayesian Inference with Anchored Ensembles of Neural Networks, and Application to Reinforcement Learning," *arXiv:1805.11324 [cs, stat]*, May 2018. [Online]. Available: <http://arxiv.org/abs/1805.11324>
- [10] A. Bry and N. Roy, "Rapidly-exploring Random Belief Trees for motion planning under uncertainty," in *2011 IEEE International Conference on Robotics and Automation*, May 2011, pp. 723–730.
- [11] M. L. Rodríguez-Arévalo, J. Neira, and J. A. Castellanos, "On the Importance of Uncertainty Representation in Active SLAM," *IEEE Transactions on Robotics*, vol. 34, no. 3, pp. 829–834, June 2018.
- [12] B. Axelrod, L. Kaelbling, and T. Lozano-Perez, "Provably Safe Robot Navigation with Obstacle Uncertainty," in *Proceedings of Robotics: Science and Systems XIII*, Cambridge, Massachusetts, USA, July 2017.
- [13] Y. Liao, L. Huang, Y. Wang, S. Kodagoda, Y. Yu, and Y. Liu, "Parse geometry from a line: Monocular depth estimation with partial laser observation," in *2017 IEEE International Conference on Robotics and Automation (ICRA)*, May 2017, pp. 5059–5066.
- [14] S. Thrun, W. Burgard, and D. Fox, *Probabilistic Robotics (Intelligent Robotics and Autonomous Agents)*. The MIT Press, 2005.
- [15] R. Valencia, J. Andrade-Cetto, and J. M. Porta, "Path planning in belief space with pose SLAM," in *2011 IEEE International Conference on Robotics and Automation*, May 2011, pp. 78–83.
- [16] L. Janson, E. Schmerling, and M. Pavone, "Monte Carlo Motion Planning for Robot Trajectory Optimization Under Uncertainty," in *Robotics Research*, A. Bicchi and W. Burgard, Eds. Cham: Springer International Publishing, 2018, vol. 3, pp. 343–361.
- [17] E. Vespa, N. Nikolov, M. Grimm, L. Nardi, P. H. J. Kelly, and S. Leutenegger, "Efficient Octree-Based Volumetric SLAM Supporting Signed-Distance and Occupancy Mapping," *IEEE Robotics and Automation Letters*, vol. 3, no. 2, pp. 1144–1151, 2018.
- [18] J. S. Denker and Y. Lecun, "Transforming neural-net output levels to probability distributions," in *Advances in neural information processing systems*, 1991, pp. 853–859.
- [19] D. J. C. MacKay, "A Practical Bayesian Framework for Backpropagation Networks," *Neural Computation*, vol. 4, no. 3, pp. 448–472, May 1992.
- [20] C. Blundell, J. Cornebise, K. Kavukcuoglu, and D. Wierstra, "Weight Uncertainty in Neural Network," in *International Conference on Machine Learning*, June 2015, pp. 1613–1622.
- [21] A. Kendall, V. Badrinarayanan, and R. Cipolla, "Bayesian SegNet: Model Uncertainty in Deep Convolutional Encoder-Decoder Architectures for Scene Understanding," *arXiv:1511.02680 [cs]*, Nov. 2015. [Online]. Available: <http://arxiv.org/abs/1511.02680>
- [22] A. Kendall and R. Cipolla, "Modelling uncertainty in deep learning for camera relocalization," in *2016 IEEE International Conference on Robotics and Automation (ICRA)*, May 2016, pp. 4762–4769.
- [23] A. Kendall and Y. Gal, "What Uncertainties Do We Need in Bayesian Deep Learning for Computer Vision?" in *Advances in Neural Information Processing Systems 30*, I. Guyon, U. V. Luxburg, S. Bengio, H. Wallach, R. Fergus, S. Vishwanathan, and R. Garnett, Eds. Curran Associates, Inc., 2017, pp. 5574–5584.
- [24] S. Ioffe and C. Szegedy, "Batch Normalization: Accelerating Deep Network Training by Reducing Internal Covariate Shift," in *PMLR*, June 2015, pp. 448–456.
- [25] K. He, X. Zhang, S. Ren, and J. Sun, "Delving Deep into Rectifiers: Surpassing Human-Level Performance on ImageNet Classification," in *2015 IEEE International Conference on Computer Vision (ICCV)*, Dec. 2015, pp. 1026–1034.
- [26] C. Loop, Q. Cai, S. Orts-Escolano, and P. A. Chou, "A Closed-Form Bayesian Fusion Equation Using Occupancy Probabilities," in *2016 Fourth International Conference on 3D Vision (3DV)*, 2016, pp. 380–388.